Development ePress online publication date 28 November 2012

Development 140, 0000-0000 (2013) doi:10.1242/dev.086215

Predicting stem cell fate changes by differential cell cycle progression patterns

Marta Roccio[1], Daniel Schmitter[1,2], Marlen Knobloch[3], Yuya Okawa[1], Daniel Sage[2] and Matthias P. Lutolf[1,*]

SUMMARY

Stem cell self-renewal, commitment and reprogramming rely on a poorly understood coordination of cell cycle progression and execution of cell fate choices. Using existing experimental paradigms, it has not been possible to probe this relationship systematically in live stem cells *in vitro* or *in vivo*. Alterations in stem cell cycle kinetics probably occur long before changes in phenotypic markers are apparent and could be used as predictive parameters to reveal changes in stem cell fate. To explore this intriguing concept, we developed a single-cell tracking approach that enables automatic detection of cell cycle phases in live (stem) cells expressing fluorescent ubiquitylation-based cell-cycle indicator (FUCCI) probes. Using this tool, we have identified distinctive changes in lengths and fluorescence intensities of G1 (red fluorescence) and S/G2-M (green) that are associated with self-renewal and differentiation of single murine neural stem/progenitor cells (NSCs) and embryonic stem cells (ESCs). We further exploited these distinctive features using fluorescence-activated cell sorting to select for desired stem cell fates in two challenging cell culture settings. First, as G1 length was found to nearly double during NSC differentiation, resulting in progressively increasing red fluorescence intensity, we successfully purified stem cells from heterogeneous cell populations by their lower fluorescence. Second, as ESCs are almost exclusively marked by the green (S/G2-M) FUCCI probe due to their very short G1, we substantially augmented the proportion of reprogramming cells by sorting green cells early on during reprogramming from a NSC to an induced pluripotent stem cell state. Taken together, our studies begin to shed light on the crucial relationship between cell cycle progression and fate choice, and we are convinced that the presented approach can be exploited to predict and manipulate cell fate in a wealth of other mammalian cell systems.

KEY WORDS: Cell cycle progression, Self-renewal, Differentiation, FUCCI, Reprogramming, Neural stem cell, Embryonic stem cell, Time-lapse microscopy, Cell tracking, Mouse

INTRODUCTION

Cell cycle progression and lineage commitment of stem cells appear to be tightly linked processes (Lange and Calegari, 2010; Orford and Scadden, 2008; Singh and Dalton, 2009). In particular, the early G1 phase of the cell cycle plays a crucial role in the differentiation of stem cells, as it represents a window of responsiveness to extrinsic cues (Blomen and Boonstra, 2007). Progression from G1 to S phase in most somatic cells requires the phosphorylation of the retinoblastoma protein (Rb) by the mitogen-dependent activity of cyclins, namely the CDK4-cyclin D and the CDK2-cyclin E complex (Harbour et al., 1999; Blomen and Boonstra, 2007). In marked contrast, Rb is hyperphosphorylated in mouse embryonic stem cells (ESCs) due to constitutive CDK2-cyclin E activity (Savatier et al., 1994; Stead et al., 2002). As a consequence, the fast cell cycle of self-renewing ESC bypasses commitment signals such as prolonged MAPK activation (Burdon et al., 1999; Burdon et al., 2002). ESCs are characterised by a very short G1 phase that makes up only about 15-20% of a cell cycle that is rather short per se (10 to 16 hours). During differentiation, G1 is markedly increased, as was shown, for example, in primate (Fluckiger et al., 2006) and human ESCs (Filipczyk et al., 2007), as well as in mouse and human induced pluripotent stem (iPS) cells (Ohtsuka and Dalton, 2008).

A similar lengthening of the cell cycle during differentiation has been observed for some somatic stem cells, including NSCs. During brain development, NSCs in the ventricular zone switch from self-renewing divisions, which expand the stem cell pool, to differentiating divisions, which give rise to neurons and committed basal progenitors (Götz and Huttner, 2005; Kriegstein and Alvarez-Buylla, 2009). These fate changes are associated with distinct kinetics in cell cycle progression: the length of G1 increases from 8 hours at the onset of neurogenesis (at E11) to 18 hours at the end (E16) (Takahashi et al., 1995). Furthermore, G1 lengthens specifically during acquisition of a neurogenic fate (Calegari et al., 2005) and during transition from apical progenitors to basal progenitors that are already committed to neuron production (Arai et al., 2011). In addition, numerous cell cycle regulators have been shown to affect stem cell fate, including cyclins and CDK inhibitors (Doetsch et al., 2002b; Kowalczyk et al., 2004; Kippin et al., 2005; Beukelaers et al., 2011). Prolongation of G1 by chemical inhibition of CDK2-cyclin E (Calegari and Huttner, 2003) or by RNAi-mediated silencing of CDK4-cyclin D (Lange et al., 2009) resulted in increased neurogenesis. By contrast, overexpression of CDK4-cyclinD led to an expansion of the progenitor pool, both during brain development (Lange et al., 2009) and in the adult hippocampus (Artegiani et al., 2011).

These and other data have led to the intriguing hypothesis that G1 lengthening is not only a consequence but can be a cause of differentiation (Götz and Huttner, 2005; Salomoni and Calegari, 2010). However, because cell cycle dynamics during stem cell fate changes have not yet been directly measured in live single stem cells, it has thus far not been possible to elucidate this bi-directional relationship in greater detail. We reasoned that a single-cell and

[1]Laboratory of Stem Cell Bioengineering, Institute of Bioengineering and School of Life Sciences, Ecole Polytechnique Fédérale de Lausanne (EPFL), Lausanne, Switzerland. [2]Biomedical Imaging Group, EPFL, Lausanne, Switzerland. [3]Brain Research Institute, Faculty of Medicine, University of Zurich, 8057 Zurich, Switzerland.

*Author for correspondence (matthias.lutolf@epfl.ch)

Accepted 22 October 2012

high-throughput analysis of dividing stem cells that undergo well-defined cell fate changes could shed light on the link between cell cycle progression and fate changes. To analyse dynamic changes in cell cycle phases, we used stem cells that express FUCCI reporters (Sakaue-Sawano et al., 2008) whose expression we automatically and precisely detected over multiple rounds of cell division by our newly developed cell tracking software termed FUCCIJ. In order to record continuously the proliferation of individual cells, we employed a previously developed microwell array technology that allows trapping of single stem cells in confined areas for long-term cell culture and exposing them to niche cues of interest (Gobaa et al., 2011; Roccio et al., 2012).

Using this combined approach, we measured a total increase in adult NSC cycle length upon induction of differentiation that was mostly caused by a doubling of G1 length. Conversely, we found that treatment of NSCs with a cell-permeable CDK4 inhibitor induced an increase in the percentage of cells in G1 and promoted differentiation. The lengthening of G1 of committed cells resulted in progressively increasing red fluorescence intensity of the G1 FUCCI reporter. We took advantage of this intensity change to separate stem cells, based on their lower red fluorescence, from more committed cells in a heterogeneous cell population using FACS. In marked contrast, owing to their very short G1, ESCs were found to be mainly marked by the green S/G2-M FUCCI reporter. We again exploited this specific change in cell cycle pattern to substantially augment the proportion of reprogramming cells by sorting green cells early on during reprogramming from a NSC to an induced pluripotent stem cell-like state. Taken together, this approach may help to overcome the heterogeneity of stem/progenitor populations that hampers many population-level *in vitro* studies.

MATERIALS AND METHODS

Mouse breeding and genotyping

C57BL/6N and DBA/2N mixed heterozygous mice expressing either Cdt1-KO2 (B6.B6D2-Tg(FUCCI)596Bsi) or Gem-AG (B6;B6D2-Tg(FUCCI)504Bsi) were obtained by the Riken Institute (Japan). Animals were crossed to obtain double positive FUCCI mice.

Isolation and culture of neural stem/progenitor cells

FUCCI mice were sacrificed by decapitation after a short isoflurane anaesthesia. Subventricular zone and whole hippocampi were dissected on ice. Four 8-week-old mice were pooled for one extraction. The two neurogenic regions were cultured separately. Cells were cultured as neurospheres as described previously (Giachino et al., 2009). Hes5::GFP cells were isolated from early postnatal brains as described previously (Giachino et al., 2009). All cells were used between P2 and P5.

Time-lapse microscopy

Time-lapse microscopy of single FUCCI cells captured in microwells was conducted as described previously (Gobaa et al., 2011; Roccio et al., 2012). Brightfield, red and green fluorescence were recorded. S/G2-M phase was measured as the time between first and last frame with green fluorescence. G1 was measured as the time between the first frame without fluorescence (after cell division) and the last frame with red fluorescence. This includes a short interval of S phase in which the cells were both green and red.

Stem cell differentiation assays

NSC differentiation on plastic dishes was performed on Laminin/Poly-L Ornithine (PLO)-coated plates in conditioned medium (from 3-day-old cell cultures). Two days later, medium was exchanged with DMEM-F12 supplemented with B27 and 2 ng/ml EGF and 2 ng/ml FGF. Cells were left in culture for 4, 6 or 10 days. Alternatively, cells were stimulated for 48 hours with 2% FBS and 1 μM retinoic acid and analysed 4 days after plating. Mouse ESC differentiation was induced by removal of LIF and addition of retinoic acid (2.5 μM).

CDK4 inhibition

The cell permeable cyclin-dependent kinase 4 (CDK4) inhibitor 2-bromo-12,13-dihydro-5H-indolo[2,3-a]pyrrolocarbazole-5,7(6H)-dione (Zhu et al., 2003) was added for 24 hours at a concentration of 1 μM to 3-day-old neurospheres that were dissociated and analysed by flow cytometry or re-plated on laminin-PLO-coated plates for differentiation assays. Alternatively, dissociated cells plated on laminin-PLO-coated plastic were treated with 1 μM CDK4i for 3 days.

Generation of a FUCCI ESC line

Mouse E14 ESC were cultured in standard condition on 0.2% gelatin-coated plates in DMEM supplemented with 15% ES-screened serum (Fisher) and 1000 U/ml LIF (Millipore). Cells were infected with FUCCI lentiviral vectors (Riken Institute, Japan) and 3 days post-infection sorted by FACS to single cells using 96-well plates. Colonies expressing green fluorescence originating from cloned red cells (and vice versa) were selected as double-transduced clones. Nine clones were characterised by flow cytometry and clone #9 was further characterised by immunostaining and time-lapse imaging.

Generation of a FUCCI Hes5::GFP line

Hes5::GFP NSC (p2) were dissociated to single cells plated in a 12-well plate (1×10^5 cells) in suspension. Cells were transduced with the Cdt1-KO2 vector, neurosphere-cultured for 4 days and transduced $KO2^+$ cells sorted, expanded and characterised by flow cytometry and immunostaining.

FUCCI-NSC reprogramming

NSC reprogramming was adapted from a published protocol (Kim et al., 2009). Lentiviruses were generated using the following plasmids: TetO-FUW-OSKM (Addgene plasmid 20321 containing Oct3/4, Sox2, Klf4 and c-Myc; for simplicity termed '4F') and with FUW-M2rtTA (Addgene plasmid 20342 containing a transactivator). Transduction efficiencies were estimated by Oct4 staining 48 hours after doxycycline (dox: 2 μg/ml) induction. To induce reprogramming, 1×10^5 FUCCI-NSC (4F line) were seeded in NSC medium in 12-well plates and grown as neurospheres. Dox was added to the medium at day 0. Three days after dox induction, neurospheres were dissociated and plated in PLL-coated plates in ESC medium in presence of LIF and dox. Colony formation was estimated at day 7 and 10. Alternatively, 3×10^5 cells were seeded on PLL-coated 10 cm dishes and induced with dox for 3 days. Three days after induction, medium was changed to ESC medium containing LIF and dox. Cells were sorted 4 days after dox induction. 1000 cells were seeded per well in 96-well plates to establish colony-forming efficiency. 10,000 cells were seeded on microwell arrays for time-lapse imaging.

Statistical analysis

Paired *t*-tests were used to evaluate the statistical significance between two groups. One way-ANOVA with a Bonferroni post-test for multiple comparisons was used when more then two groups were compared. Differences in segregation in synchronous and asynchronous cell divisions were evaluated using a Pearson's Chi square test.

RESULTS

Automated cell cycle phase analysis of single FUCCI-stem cells

Dynamic analysis of cell cycle progression by live-cell imaging has become feasible with the generation of the FUCCI reporter system (Sakaue-Sawano et al., 2008). To automatically and precisely detect cells based on the fluorescence of the two FUCCI reporters and to reconstruct genealogical trees of dividing cells, we developed a novel cell-tracking software as an ImageJ plug-in package (termed FUCCIJ) that allows extracting cell cycle phase lengths, fluorescence intensities, cell positions and finally entire lineage trees of single cells (Fig. 1; supplementary material Fig. S1; Movies 1, 2). FUCCIJ is delivered as two independent ImageJ plugins termed 'Cell Lineage' and 'Tree Lineage'. After a preprocessing and filtering step automatic cell detection is

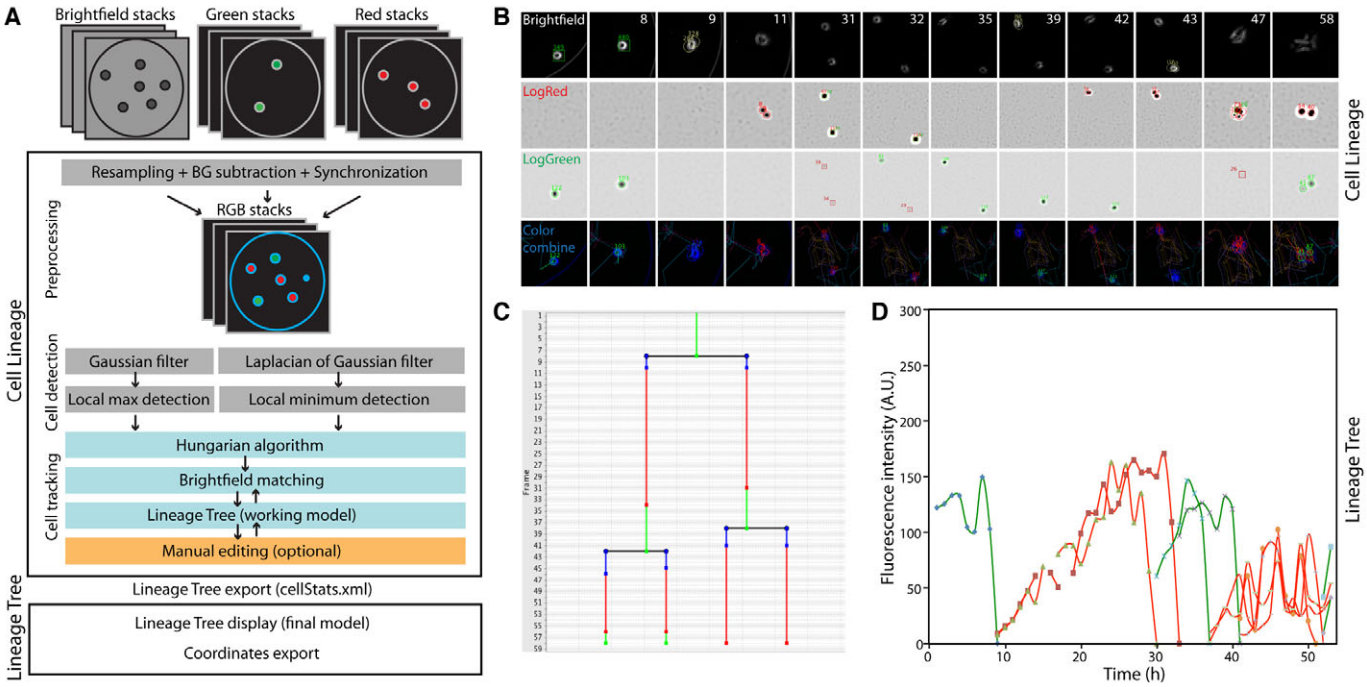

Fig 1. Automated analysis of cell cycle phases in single stem cells. (**A**) The FUCCIJ software with two independent ImageJ plug-ins: 'Cell Lineage' and 'Lineage Tree'. (**B**) Example of still images from a time-lapse experiment with FUCCI-NSC detected and displayed by FUCCIJ. (**C**) Lineage tree for the same cell displayed in B is shown with the FUCCI colour code. (**D**) Fluorescence intensity at each time point is extracted and plotted for the same cell displayed in B and C. Red line, G1; green line, S/G2-M.

performed. User-based editing allows correction of false-positive or false-negative detections. Lineage tree generation is based on the Hungarian algorithm as well as on custom-made combinatorial and probabilistic models in which theoretical expectations are combined with the results of detection.

To analyse stem cell cycle dynamics at single-cell level and with high temporal resolution and throughput, we trapped cells in hydrogel microwell arrays for time-lapse microscopy (Gobaa et al., 2011; Roccio et al., 2012) (supplementary material Fig. S1A). Individual microwells can be functionalized with desired biomolecules in order to expose cells to components of their native micro-environment (e.g. laminin1).

Isolation and characterisation of adult FUCCI-NSC

As a first model system to try to unveil the relationship between cell cycle progression and fate choice-making, we isolated adult neural stem and progenitor cells (for simplicity herein termed 'NSCs') from the subventricular zone (SVZ) and dentate gyrus (DG) of 8-week-old FUCCI mice. Under normal physiological conditions *in vivo*, we detected cycling (i.e. green; S/G2-M) cells in the SVZ and DG by confocal analysis of brain sections (supplementary material Fig. S2A). Lower numbers of green cells were found in DGs, indicating fewer cycling cells (Abrous et al., 2005). We isolated NSCs based on their neurosphere-forming capacity in medium containing EGF and FGFb from both neurogenic areas, but focused on SVZ-derived neurosphere-forming cells for subsequent *in vitro* characterisation.

Immunostaining revealed that 80-100% of the obtained cells were positive for the stem and progenitor cell markers Nestin (98.5±0.7%) and Sox2 (84±8%) (Fig. 2A). Flow cytometry analyses showed that the population contained 48.7±1.5% Cdt1-KO2-positive ($KO2^+$) cells (red), 19.8±4.1% Gem-AG-positive (AG^+) (green), 2.5±1.2% double-positive and 28.2±5.3% double-negative cells (Fig. 2B,C). These proportions were comparable for two independent SVZ isolations. Furthermore, no difference in cell cycle phase distribution was observed between cells growing as neurospheres compared with adherent culture conditions. DG-derived cells showed similar proportions of the four subpopulations (supplementary material Fig. S2B); however, in this case we detected a higher percentage of G1 when cells were cultured as spheres. To quantify the percentage of cells in mitosis (M), we immunostained cells for the mitotic marker phospho-S10-H3 and found that ~5% of the cells stained positive (supplementary material Fig. S2C).

DNA staining using Hoechst confirmed that Cdt1-$KO2^+$ cells represent a population of cells in G1 (2n cells), whereas Gem-AG^+ cells contain twice the amount of DNA (4n cells) and intermediate amounts and are therefore in S/G2-M (Fig. 2B). Double-positive cells with intermediate DNA amounts mark cells at the onset of S phase. The double-negative population represented primarily 2n cells with a smaller percentage of 4n-cells (~10%). FACS of the double-negative population and flow cytometry analysis after 4 days in culture, showed that 90% of the double-negative population consisted of cells that regained fluorescence in culture (supplementary material Fig. S3). This was also confirmed by time-lapse microscopy where ~90% of the non-fluorescent cells reacquired red fluorescence within 2 to 3 hours of cytokinesis and regained green fluorescence upon cell cycle progression, whereas the remaining 10% of initially double-negative cells expressed only the red fluorescent protein. Therefore, the majority of double-negative cells are early G1 cells.

Imaging of single cells over 3 days allowed recording of approximately three consecutive cell divisions. Clone formation was very efficient, as 71±10% of all single cells proliferated

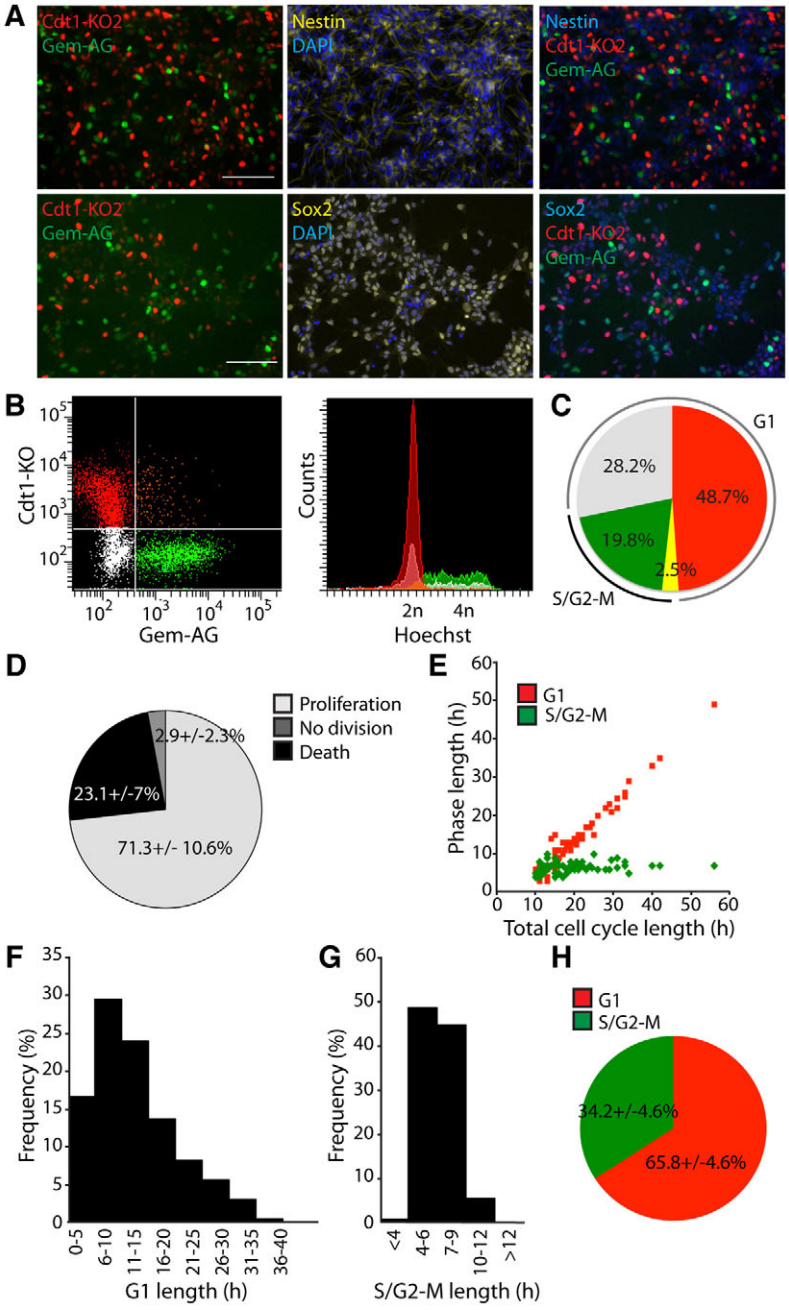

Fig 2. Cell cycle analysis of single FUCCI-NSC. (**A**) FUCCI-NSC isolated from SVZ and plated on laminin-PLO substrates stained for Nestin, Sox2 and with DAPI. Scale bars: 100 μm. (**B**) Cell cycle analysis by flow cytometry of FUCCI-NSC co-stained with Hoechst and (**C**) quantification of four sub-populations: Cdt1-KO2$^+$ (red), Gem-AG$^+$ (green), double-positive (yellow) and double-negative (grey). Averages of six samples of consecutive passages are shown. (**D**) Quantification of cell fates of single FUCCI-NSC in microwell arrays followed by time-lapse microscopy for 3 days (*n*=6 experiments with a minimum of *n*=50 cells per experiment, ±s.d.). (**E**) G1 (red) and S/G2-M (green) length of single FUCCI-NSC as a function of entire cell cycle. (**F**) Distribution of G1 (*n*=273 segments). (**G**) Distribution of S/G2-M (*n*=256). (**H**) Relative percentages of time spent in G1 and S/G2-M calculated for each experiment (*n*=6, ±s.d.).

extensively (Fig. 2D), indicating no phototoxicity despite prolonged fluorescence image acquisition. A small percentage of cells (2.9±2.3%) never divided during the 3-day experiment, and the remaining cells (23±7%) died at different time points during acquisition. Using FUCCIJ, we quantified the cell cycle characteristics of these cells at single cell level. We observed a remarkably broad distribution of the times taken by mother NSC to enter the first division (supplementary material Fig. S4A). This was primarily dependent on a similarly broadly distributed G1, whereas S/G2-M was relatively homogeneous (Fig. 2E-G). The average duration of G1 and S/G2-M phase was 12±7 and 6.6±1.6 hours, respectively. Notably, we observed a shortening of the cell cycle and G1 in consecutive divisions (supplementary material Fig. S4B). Overall, this resulted in G1 representing 66% of the total cell cycle, whereas S/G2-M made up 34% (Fig. 2H), matching the ratios determined by flow cytometry above.

Induction of differentiation results in G1 lengthening and more asynchronous divisions

To elucidate whether cell fate changes are linked to distinct changes in cell cycle progression, we compared G1 and S/G2-M in FUCCI-NSC cultured for 4 days under self-renewal conditions or differentiation-initiating conditions induced by growth factor withdrawal (Fig. 3). An end-point analysis showed a 1.3-fold increase in Cdt1-KO2$^+$ cells (red), and a concomitant ~60% decrease in the percentage of Gem-AG$^+$ cells (green) in adherent cultures (Fig. 3A) and neurospheres (data not shown) upon growth factor withdrawal. Immunostaining of the mitotic marker phospho-S10-H3 also confirmed the significantly lower numbers of mitotic cells under differentiation-initiating conditions (1.1±0.5%) compared with self-renewal (5.7±2%) (supplementary material Fig. S5). Furthermore, Nestin expression was markedly reduced and we detected a significant

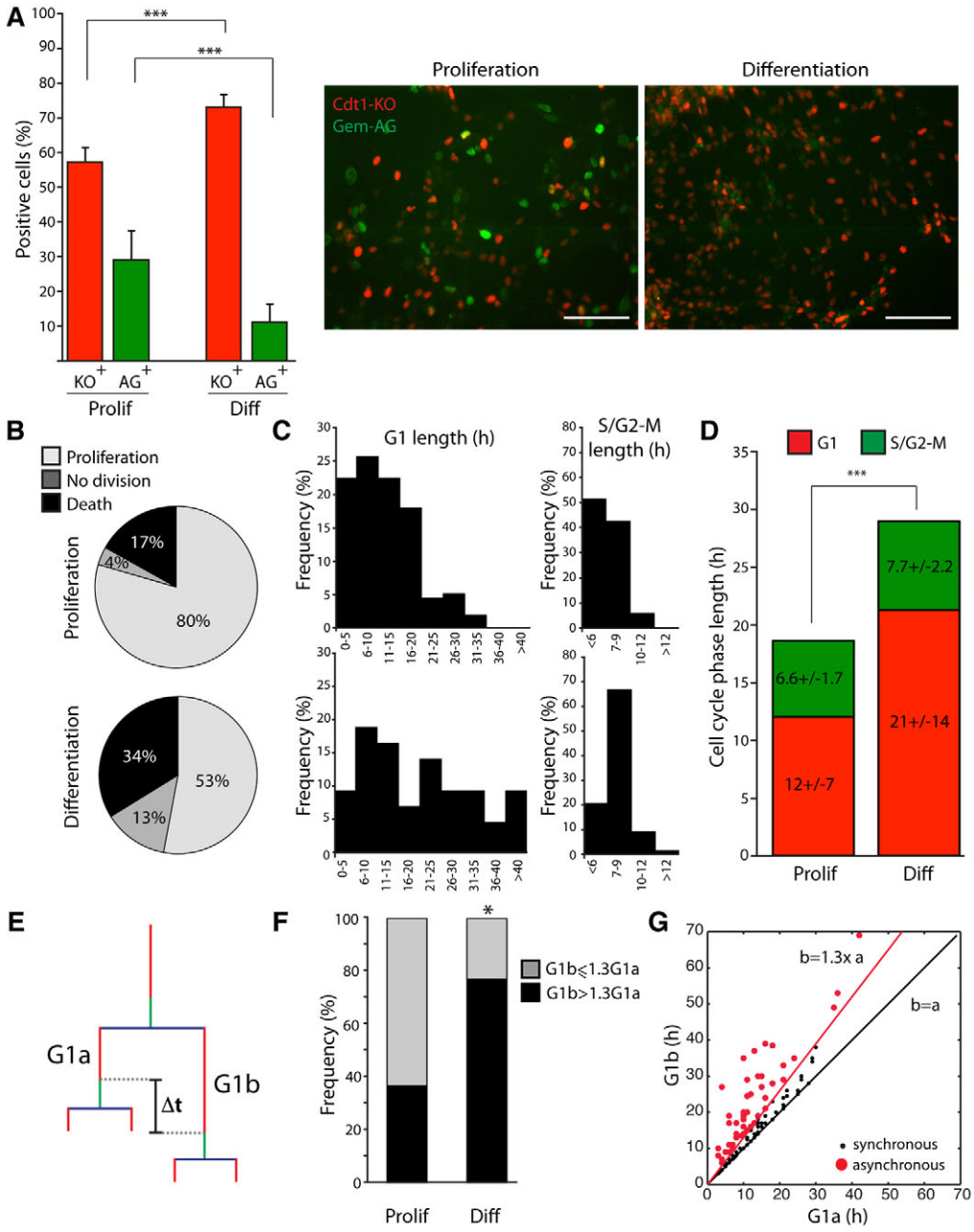

Fig 3. Differentiation prolongs G1 in FUCCI-NSC. (**A**) Quantification of Cdt1-KO$^+$ and Gem-AG$^+$ cells (normalized to DAPI) under proliferation and differentiation (±s.d.; ***P<0.001). A representative example is shown on the right. Scale bars: 100 µm. (**B**) Quantification of single cell fates under proliferation and differentiation (n=6 independent experiments). (**C**) Distribution of G1 and S/G2-M length (G1prolif, n=150; G1diff, n=42; S/G2-Mprolif, n=135; S/G2-Mdiff, n=52). (**D**) Quantification of average length of each phase. (**E**,**F**) Frequency of asynchronous cell divisions using a dynamic threshold with Δt corresponding to 30% of the total cell cycle length of daughter cell 'a' (G1b>1.3G1a). (**G**) G1a and G1b plotted for proliferative and differentiation divisions (n=123 pairs). Asynchronous divisions (G1b>1.3G1a) indicated in red.

increase in the expression of astrocytic (marked by GFAP) and neuronal fates (βIII-tubulin). After 10 days of differentiation, neurons made up 11.8±4.6%, oligodendrocytes 0.7±0.7% and astrocytes 38.4±14.7% of the population (supplementary material Fig. S6). In all cases, terminally differentiated cells displayed red fluorescent nuclei as expected.

To analyse the dynamics of single cell cycle progression during differentiation initiation, we continuously filmed cells for 3 days. Growth factor withdrawal caused a marked reduction in cell proliferation, as well as an increase in cell death (Fig. 3B). We also detected an increase in the percentage of non-dividing cells (4-13%), suggesting that these cells terminally differentiated. For 60% of the dividing cells, only one division occurred within 3 days and it was not possible to evaluate the duration of G1, as red fluorescence was maintained till the end of the experiment. Similar results were obtained in a 4-day time-lapse experiment (data not shown). It is therefore likely that these cells have exited the cycle and are on their way to terminal differentiation. In agreement with this, 85% of all cells cultured in the presence of growth factors were positive for Ki67, whereas after 4 days in low growth factors

conditions, the percentage of Ki67-positive cells was reduced to 45% (data not shown). For 40% of cells that divided a second time within 3 days, we observed a significant increase in G1 from 12±7 to 21±14 hours (Fig. 3C,D). Concomitantly, we also observed a minor but significant increase in the duration of S/G2-M from 6.6±1.7 to 7.7±2.2 hours. Therefore, differentiation is accompanied by cell cycle lengthening, which may precede exit from the cell cycle.

To extract information on the synchrony of cell divisions, we analysed the difference in the length of G1 of the first generation of sister cells (Δt=G1a–G1b) (Fig. 3E). We defined divisions as asynchronous when the length of G1 of the paired daughters differed by more than 30%. Interestingly, the percentage of asynchronous divisions more than doubled when cells were moved from self-renewal to differentiation-inducing conditions (36.6 versus 76.9%) (Fig. 3F). The overall ratio of synchronous versus asynchronous divisions did not vary with increasing cell cycle length, whereas the percentage of synchronous divisions (Δt=0) dropped with increased cell cycle duration. Twenty three percent of cells with an average G1 shorter than 19 hours (average + 1 s.d.) showed this behaviour, whereas only 9.6% divided synchronously in cells with extended G1 (G1>19 hours) (Fig. 3G).

Forced G1 lengthening by chemical inhibition of CDK4 increases differentiation

The marked increase in G1 length observed upon initiation of differentiation led us to design an inversed experiment to understand whether forced lengthening of G1 by chemical inhibition of CDK4 could influence NSC differentiation. In neurospheres or adherent cells treated with different concentrations of a cell-permeable CDK4 inhibitor (CDK4i), we detected an increase in the proportion of $KO2^+$ cells (red) at the concentration of 1 μM (supplementary material Fig. S7A). Using a standard 10-day differentiation protocol, inhibition of CDK4 resulted in an approximate twofold increase in the number of neurons (supplementary material Fig. S8B, Fig. S7E), and a ~30% decrease in the percentage of GFAP-positive cells (supplementary material Fig. S8B-D). However, we also measured ~50% reduction (P<0.001) in the total number of cells in samples treated with CDK4i (supplementary material Fig. S8A), likely caused by cytotoxic and cytostatic effects exerted by this inhibitor (Sakaue-Sawano et al., 2011; Zhu et al., 2003). Therefore, in order to exclude effects related to differences in cell numbers (e.g. paracrine signals, differential cell-cell contacts or GF consumption), we assessed cultures after just 4 days of CDK4i-treatment where cultures were not confluent and cell numbers were comparable. Indeed, we detected a significant increase in $KO2^+$ cells from 60±1.1 to 67±0.3%, as well as an increased fluorescence intensity compared with untreated cells (Fig. 4A). Furthermore, immunostaining showed an increase in the expression of βIII-tubulin in CDK4i-treated cells (Fig. 4B). As the large majority of these cells still expressed Nestin at this early time point, we believe that these cells are neuroblasts rather than neurons.

Next, we used the FUCCI system in combination with FACS to synchronize the population by sorting G1 cells and induce differentiation, either by growth factor withdrawal or by the addition of serum and retinoic acid (RA), specifically during G1 in $KO2^+$ cells (Fig. 4C). As expected, we observed a more pronounced differentiation induction by addition of serum/RA compared with low growth factor conditions. CDK4i pretreatment induced a twofold increase in βIII-tubulin (Fig. 4D) and GFAP (Fig. 4E) expression in low growth factor conditions, and a 1.7-fold induction in presence of serum/RA compared with untreated cells, as shown by flow cytometric analysis. Interestingly, the percentage of $KO2^+$ cells correlated with the percentage of differentiated cells in an exponential fashion, both in the case of GFAP expression and βIII-tubulin (Fig. 4F,G). These data show that the prolongation of G1 by chemical inhibition of CDK4 results in increased differentiation.

Differences in red FUCCI fluorescence intensities mark distinct NSC states

Owing to the fact that fluorescent protein expression in the FUCCI system is driven by a constitutively active CAG promoter and solely regulated by expression of the respective E3 ligases (APC^{Cdh1} and SCF^{Skp2} complexes), we reasoned that prolonged cell cycle phases would result in continuously increasing fluorescence intensity and that differences in fluorescence intensities might be used to distinguish different stem cell fates. Using FUCCIJ, we were able to precisely extract fluorescence intensity values of each cell at any time point and thus could directly test this. Indeed, cells that never divided constantly accumulated the red fluorescent protein (Fig. 5A). By marked contrast, dividing cells reached a lower maximum fluorescence intensity that linearly correlated with G1 (Fig. 5B), suggesting that differentiating cells have a distinctively higher expression of the red fluorescent protein. In addition, flow cytometry data showed that not only the percentage of Cdt1-$KO2^+$ increases upon differentiation, but also the intensity of red fluorescence (Fig. 5C).

To corroborate these observations, we analysed by flow cytometry a heterogeneous population of partially differentiated cells. We found that cells expressing the neuronal marker βIII-tubulin belonged to the cell population expressing higher levels of the KO2 reporter (‘high-red’ population) (Fig. 5D,F). Conversely, Nestin- and EGFR-positive cells were mainly found in the population comprising lower red fluorescence (‘low-red’) (Fig. 5E,F). Similar results were obtained for differentiation induced by CDK4i treatment, both in the absence of growth factors or the presence of serum/RA (supplementary material Fig. S9). In all conditions examined, we observed on average a twofold enrichment in differentiated cells in the high-red compared with the low-red cells (supplementary material Fig. S9A,B), and an approximately linear correlation between the percentage of differentiated cells and the intensity of the red fluorescent protein marker (supplementary material Fig. S9C). Importantly, the same was also true in normally proliferating cells, where by qRT-PCR we identified in the high-red population a lower expression of stem cell markers and higher expression levels of differentiation markers (supplementary material Fig. S10). High-red cells also displayed an increased cell size compared with low-red cells. This could be explained either by an increase in cell size of morphologically differentiated cells (neurons, astrocytes and oligodendrocytes) or by an increase in cell size during the length of the cell cycle, as S/G2-M cells are larger than G1 cells (supplementary material Fig. S11A,B).

Enriching for NSCs in heterogeneous populations based on distinct cell cycle parameters

Heterogeneous stem cell populations despite identical growth conditions are a problem in many stem cell areas and distinct markers are often lacking that separate stem cells from already committed cells. To test whether differences in red fluorescence could be further exploited to enrich stem cells in heterogeneous cell populations, we first sorted cells by FACS based on the 20% highest and 20% lowest red fluorescence intensities, and re-plated

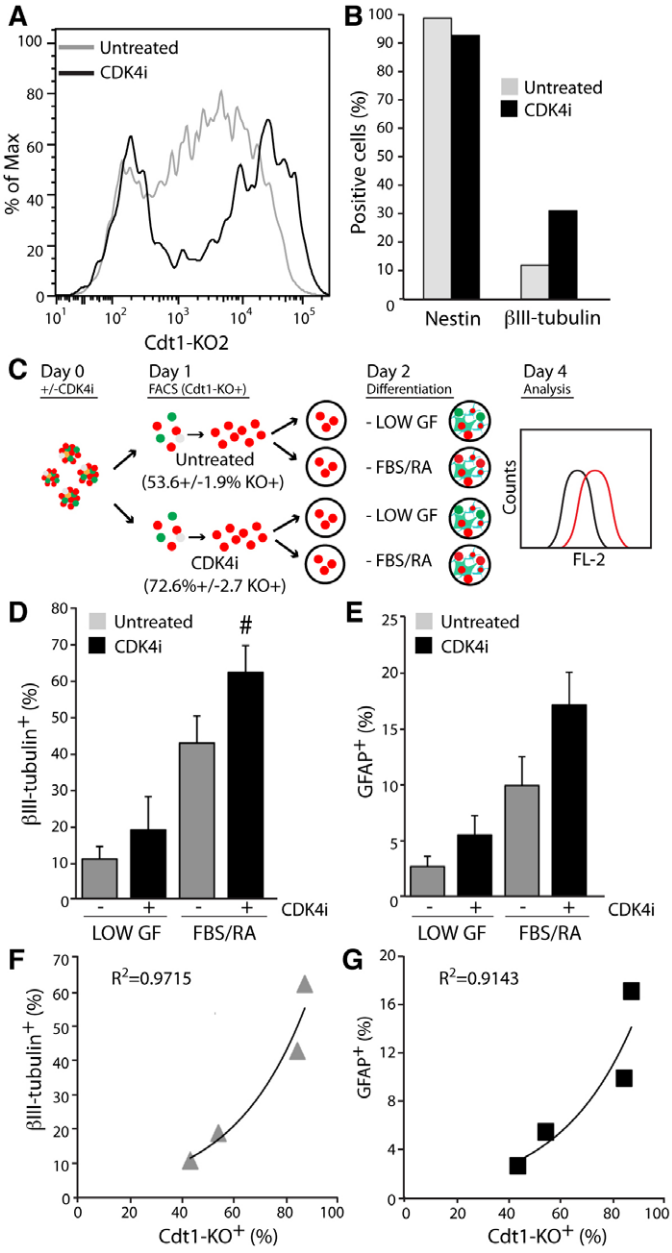

Fig 4. Forced G1 lengthening induces differentiation of FUCCI-NSC. (**A**) Cdt1-KO$^+$ levels measured by flow cytometry in untreated and CDK4i-treated cells. (**B**) Percentage of Nestin and βIII-tubulin-positive cells at day 4 (representative example of n=3). (**C**) Schematic of experiment to induce differentiation on synchronized G1 cells. (**D**,**E**) Quantification of (D) βIII-tubulin$^+$ and (E) GFAP$^+$ cells (n=4, mean±s.d.; $^*P$<0.05, $^\#P$=0.053). (**F**,**G**) Average percentage of Cdt1-KO$^+$ cells as a function of average percentage of (F) βIII-tubulin$^+$ or (G) GFAP$^+$ cells. Exponential fittings with R^2 are indicated.

them under differentiation conditions in low growth factor medium for 3 days. Directly after sorting, Nestin-positive cells were found to be ~1.6-fold more abundant in the low-red population that also comprised 30% fewer βIII-tubulin-expressing cells (not shown). Furthermore, the number of cells recovered from the high-red population after 3 days was more than three times lower (P<0.001) (supplementary material Fig. S11C), showing that cells with higher fluorescence have a reduced proliferation rate in accordance with their committed state. Nevertheless, upon differentiation for 5 days, both cell populations were able to give rise to neurons and astrocytes to a comparable extent (supplementary material Fig. S11D).

To verify if fast-cycling (i.e. low red) cells indeed represent a population of neural stem cells, we took advantage of NSC isolated from Hes5::GFP transgenic mice (Basak and Taylor, 2007; Lugert et al., 2010). In this model, GFP expression reports Notch activity and was used to identify stem cells both during embryonic development and in the adult mouse brain. In addition, we have previously shown that neurosphere generation on laminin 1-functionalized hydrogel substrates is higher in cells expressing high levels of GFP (Roccio et al., 2012). Here, we examined the cell cycle progression of Hes5::GFP cells in greater detail.

Low GFP expressing cells showed a significant reduction in proliferation, as 91±8% of these cells were in G1/G0, in contrast to 75±2% of cells expressing high GFP levels (Fig. 5G). Hes5::GFP cells expressing the red FUCCI reporter construct Cdt1-KO2 showed similar cell cycle profiles to the parental cells with ~75% of the cells being Cdt1-KO2 positive (Fig. 5H) and are tripotent, as confirmed by immunostaining (Fig. 5I). The remaining 10% of G1 cells did not express the reporter, suggesting they are early G1 cells. Under self-renewal conditions, where the majority of cells retained GFP expression (80%), we detected GFP-negative cells exclusively in cells expressing the highest levels of the red reporter (Fig. 5J,K). By contrast, high GFP cells were enriched in the S/G2-M population (Fig. 5L). These data show that it is indeed possible to further subdivide NSCs grown under identical conditions based on their cell cycle progression, with the fast-cycling cells in heterogeneous NSC cultures comprising stem or progenitor cells, and cells with increased G1 length being already committed.

Self-renewing ESCs are predominantly green and double their G1 phase upon induction of differentiation

An even more heterogeneous and rare stem cell fate change occurs during the process of reprogramming of somatic cells into induced pluripotent stem (iPS) cells, a process that is well known to be accompanied by dramatic changes in cell cycle progression (Smith et al., 2010). We wondered whether it would be possible to augment reprogramming by selecting cells with a specific cell cycle pattern.

We first analysed cell cycle progression patterns of FUCCI mouse embryonic stem cells (FUCCI-ESC) that we generated by lentiviral transduction and clonal expansion of wild-type E14 cells (Fig. 6; supplementary material Fig. S12). Under self-renewal conditions in the presence of LIF, FUCCI-ESC maintained expression of alkaline phosphatase, Nanog (supplementary material Fig. S12A,B) and Oct4 (not shown). FUCCI-ESC colonies displayed very high levels of green fluorescence (Fig. 6A-C) and when examined by flow cytometry, only 6±2.9% of the cells expressed the red G1 reporter. 54.9±1.7% of the population were Gem-AG positive, whereas 35.7±3% were double negative. Based on DNA profile, BrdU and phospho-S10-H3 staining (supplementary material Fig. S12C-E), we confirmed that red cells are predominantly in G1 (88%) and green cells in S/G2-M (84%). The blank population represented 65% of cells in G1 and 35% in S/G2-M. We believe that this is caused by rapid cycling, not allowing accumulation of the FUCCI constructs.

We next monitored by time-lapse microscopy changes in cell cycle progression during ESC commitment induced by LIF removal (Fig. 6D,E; supplementary material Fig. S12F-H). Under self-

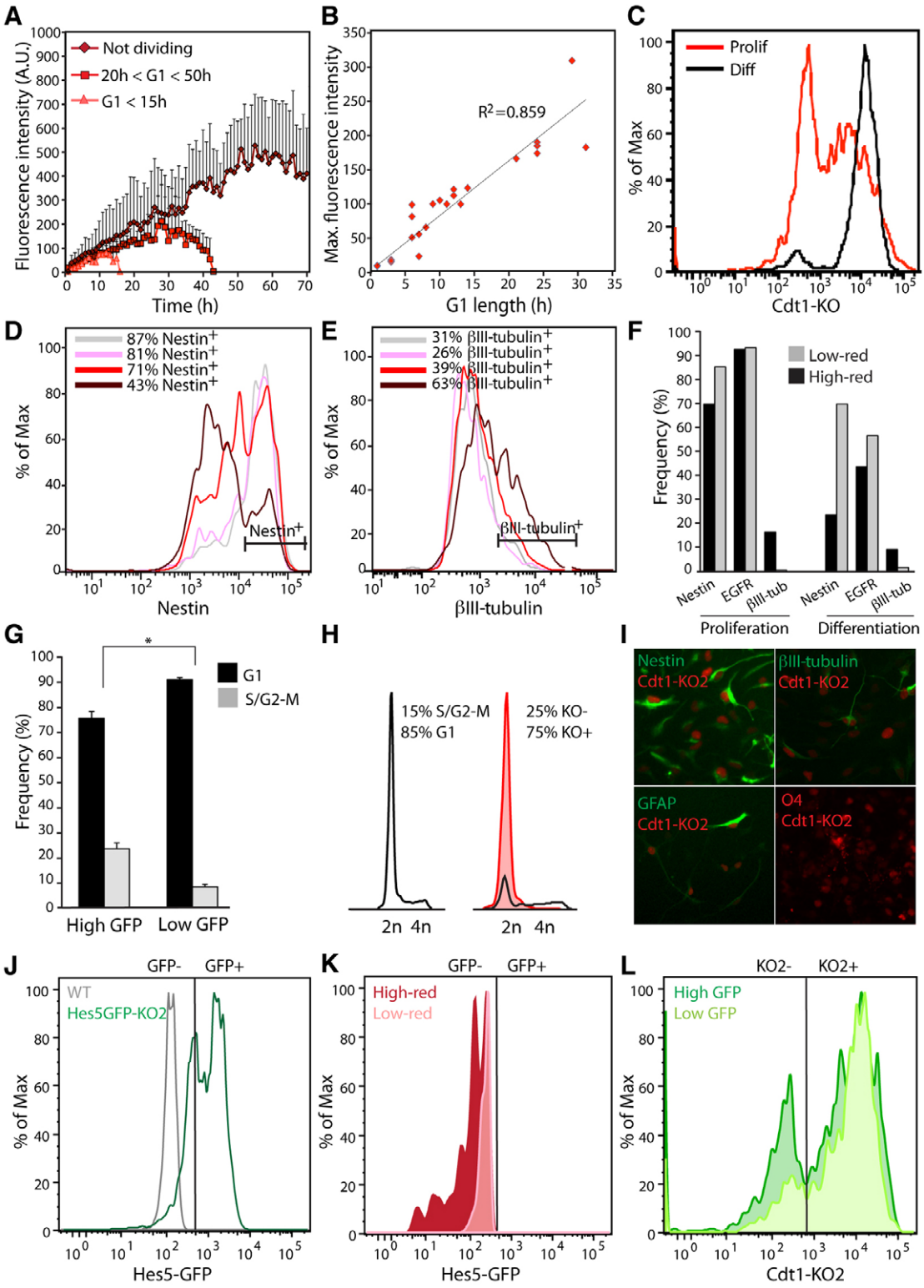

Fig 5. Purification of neural stem cells from heterogeneous populations by differential cell cycle progression. (**A**) Quantification of red fluorescence intensities of single cells with different cell cycle kinetics (n=6, ±s.d.). (**B**) Maximal red fluorescence for a given G1 length. Linear fitting and R^2 are indicated. (**C**) Red fluorescence intensity quantified by flow cytometry in proliferating and terminally differentiated cells after 10 days of differentiation (representative example). (**D**,**E**) Expression of βIII-tubulin (D) and Nestin (E) in partially differentiated FUCCI cells after 4 days of differentiation. (**F**) Quantification of surface markers by flow cytometry in the 20% lowest and highest red fluorescent cells (representative example). (**G**) Cell cycle analysis of Hes5::GFP cells on 10% lowest and highest GFP-expressing cells (mean±s.d.; *P<0.05). (**H**) Cell cycle analysis of parental Hes5::GFP line and Hes5::GFP-Cdt1-KO2 cells. (**I**) Hes5::GFP-Cdt1-KO2 immunostained for Nestin and upon differentiation for βIII-tubulin, GFAP and O4. (**J**) Flow cytometric analysis of Hes5::GFP-Cdt1-KO2. Broken line indicates GFP$^+$ gate based on wild-type cells (grey line). (**K**,**L**) GFP expression in low and high red population (K), and Cdt1-KO2 expression in low and high GFP-expressing cells (L).

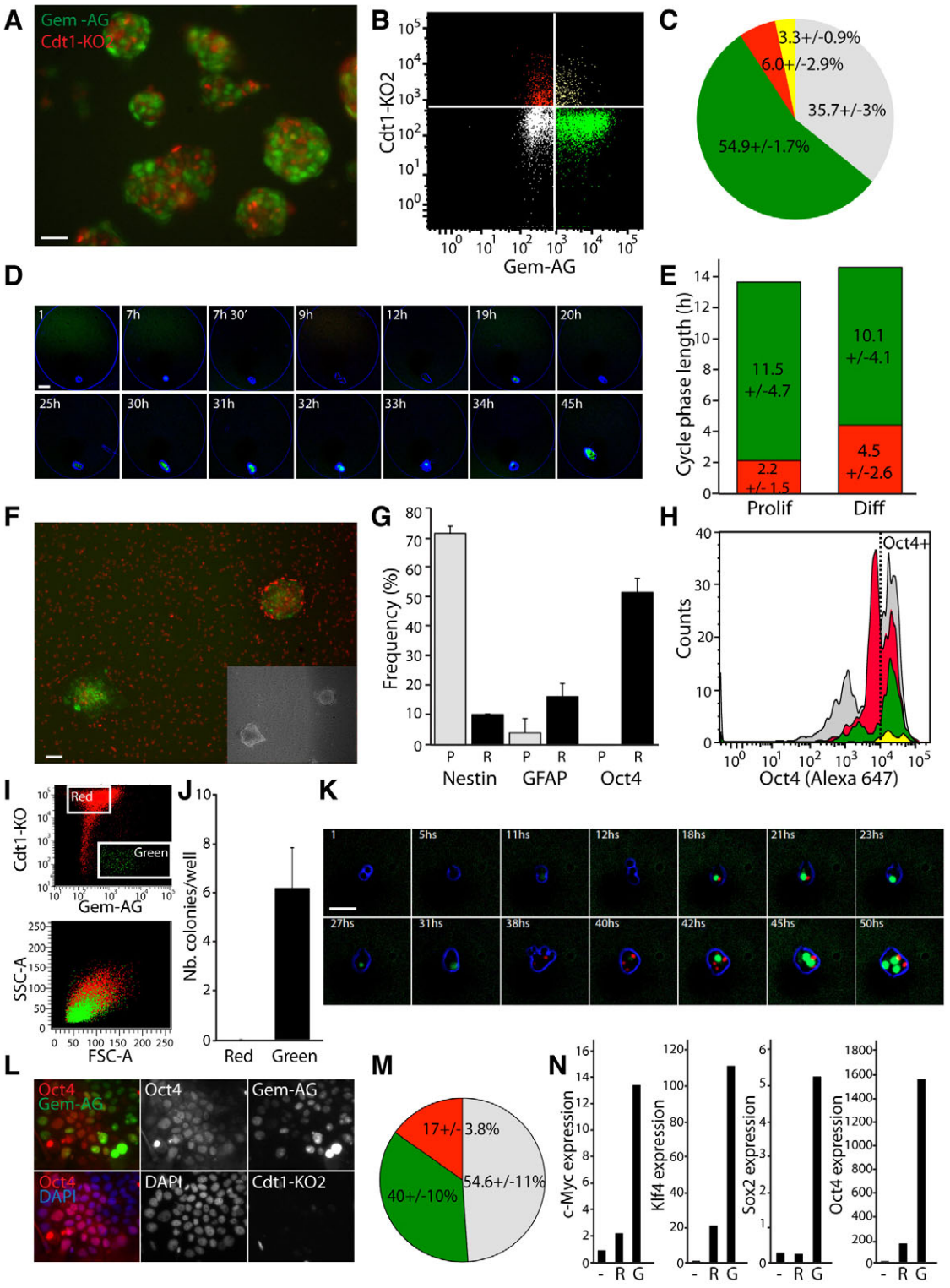

Fig 6. Enhancing reprogramming by sorting for cells in S/G2-M (green). (**A**) Representative FUCCI-ESC colonies growing in presence of LIF. Scale bar: 100 μm. (**B**,**C**) Flow cytometry of FUCCI-ESC (B) and quantification of FUCCI reporters (C) (*n*=3). (**D**) Time-lapse of single FUCCI-ESC generating a colony. (**E**) Quantification of G1 and S/G2-M length (of first two cell cycles) of FUCCI-ESC under proliferation and differentiation. (**F**,**G**) Image (F) and flow cytometric analysis (G) of 4F-transduced FUCCI-NSC 10 days after dox addition. Scale bar: 100 μm. P, 4F transduced in proliferative NSC medium –dox; R, 4F transduced 10 days +dox. Data are mean±s.d. (**H**) Oct4 expression levels obtained by flow cytometry for $KO2^+$, AG^+, double-positive and double-negative cells. Dashed line indicates $Oct4^+$ cells. (**I**) FACS scheme for red and green cells 4 days after dox treatment. (**J**) Quantification of colony numbers per 1000 sorted cells. Data are mean±s.d. (**K**) Time-lapse recording of green-sorted cells imaged in microwell arrays. (**L**) Representative images of Oct4-stained colonies seven days after sorting. (**M**) Quantification of the relative expression of Gem-AG, Cdt1-KO2 per Oct4-positive colony. (**N**) qRT-PCR for the 4F in colonies grown for 6 days from red- or green-sorted cells. –, 4F transduced in proliferative NSC medium –dox; R, red sorted; G, green sorted. All values are relative to the expression in non-transduced FUCCI-NSC.

renewal conditions, FUCCI-ESC cycle very fast through G1 (2.2±1.5 hours), whereas upon differentiation induction, the length of G1 was found to double (4.5±2.6 hours, $P<0.0001$) within only the first two cell cycles (Fig. 6E). This striking change in ESC cycle progression patterns was indeed promising for using the FUCCI reporter system to increase the efficiency of reprogramming.

Exploiting the FUCCI system to enhance reprogramming of NSC to an iPS cell-like state

We first characterised the reprogramming of FUCCI-NSC generated by transduction of doxycyclin (dox)-inducible c-Myc, Klf4, Sox2 and Oct4 (for simplicity termed '4F') using a polycistronic lentiviral vector (Carey et al., 2009; Kim et al., 2009; Kim et al., 2008) (supplementary material Fig. S13A,B). Transduction efficiency, calculated by flow cytometry from staining of Oct4 expression 48 hours after dox induction, was 27.5±8% (supplementary material Fig. S13C). Concomitantly, we detected an upregulation of c-Myc, Klf4, Sox2 and Oct4 at the mRNA level (supplementary material Fig. S13D).

Seven days after dox induction, colonies appeared that showed ESC-like morphology and displayed expression of the green FUCCI reporter that is indicative of highly proliferative clones (Fig. 6F). Efficiency was estimated as 0.9±0.7% with 4.7±5% of green cells at day 7 and 17.4±1.6% at day 10. Flow cytometric analysis revealed a dramatic decrease in Nestin expression from 71±2.5% to 10.5±0.2%, and an increase of Oct4 expression from 0.05±0.07% to 51.8±4.8% (Fig. 6G). Red cells were positive for the astrocytic marker GFAP (supplementary material Fig. S13E), whereas green and double-negative cells were positive for Oct4 (Fig. 6H; supplementary material Fig. S13E). In agreement with the above observation that green cells mark fast proliferating clones, these cells showed a reduced cell volume compared with red cells in G1. In the presence of mouse ESC medium containing FBS, only the reprogrammed clones continue to proliferate, whereas non-transduced and not reprogrammed cells differentiate and accumulate the red fluorescent reporter.

We took advantage of the underlying changes in cell cycle profiles and FUCCI reporter expression to sort cells by FACS early on during reprogramming. To this end, red and green cells were sorted 4 days after induction with dox (Fig. 6I, see scheme in supplementary material Fig. S13F). Strikingly, colony formation was detected only in the green-sorted population (Fig. 6J) with a colony-forming efficiency of ~2.4±0.7%. Early selection of fast proliferating cells allowed us to enrich the number of reprogramming cells by at least 2.5-fold, an enrichment that enabled the continuous imaging of the reprogramming process at single cell level in microwell arrays (Fig. 6K). The majority of the proliferating green-sorted cells underwent nevertheless only one cell division (supplementary material Fig. S13F, upper panel). By contrast, red-sorted cells rarely divided during the time-lapse experiment (supplementary material Fig. S13F, lower panel). Ten days after sorting, Oct4-positive colonies were identified (Fig. 6L) and a cell cycle phase distribution of the FUCCI reporters similar to the one of ESC (Fig. 6C), with 17±3.8% red, 40±10% green and 54.6±11% blank cells, was measured (Fig. 6M). Finally, we examined the expression levels of the four reprogramming factors by qRT-PCR after 6 days from red- or green-sorted cells and observed a relative increase in expression by sixfold for c-Myc, fivefold for Sox2, 20-fold for Sox2 and 10-fold in the case of Oct4 (Fig. 6N). Colonies were further clonally expanded in the absence of dox for 15 days. The cell cycle profile, quantified by flow cytometry via Hoechst labelling, and the distribution of the FUCCI reporters was undistinguishable from the one of FUCCI-ESC (supplementary material Fig. S13G). These data show that the expression of the green FUCCI reporter, which appears in a rare subpopulation of cells early after induction of reprogramming, allows the enrichment of a cell population with highly proliferative capacity and expression of pluripotency factors.

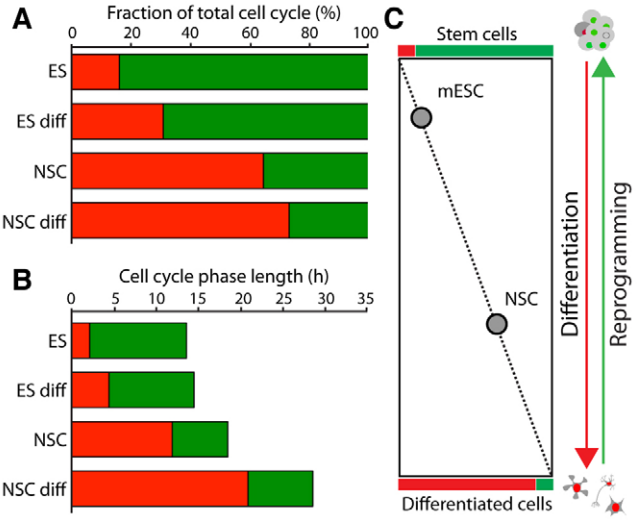

Fig. 7. Summary of time-lapse data of FUCCI-ESC and FUCCI-NSC grown in proliferation and differentiation condition.
(**A**) Percentage of time spent in G1 over the entire cell cycle is indicated in red and S/G2-M in green. (**B**) Cell cycle phase in hours for the same condition. (**C**) Proposed working model: increasing time spent in G1 is indicative of increased commitment level. Shortening of cell cycle and increase in S/G2-M phase is indicative of a more primitive cell state and can be used to identify early steps in reprogramming.

Therefore, by mapping G1 and S/G2-M phases of single NSC and ESC undergoing self-renewal and differentiation, distinct cell cycle progression patterns can be identified that are indicative of different developmental stages of these cells (Fig. 7). The knowledge on the link between cell cycle progression and cell fate choice-making can be used, as shown here for example, to enrich for stem cells in heterogeneous populations or to isolate rare cells that undergo reprogramming. These findings may also help to elucidate the relationship between cell cycle progression, differentiation and reprogramming in other cellular systems.

DISCUSSION

By taking advantage of a powerful combination of high-throughput single cell culture on an established microwell array system (Cordey et al., 2008; Gobaa et al., 2011; Roccio et al., 2012), the FUCCI reporter system (Sakaue-Sawano et al., 2008) and a newly developed single cell tracking tool (FUCCIJ), we have systematically addressed how cell cycle parameters change during self-renewal, commitment and reprogramming.

Continuous imaging of NSC isolated from FUCCI reporter mice revealed a marked heterogeneity in cell cycle duration, mostly owing to large variations in the length of G1. We also detected a significant increase in total cell cycle length and the length of G1 upon differentiation. Previous studies had already highlighted a link between G1 lengthening and differentiation during embryonic brain development. To study the link between cell cycle progression and cell fate in adult NSC, we treated FUCCI-NSC with a CDK4 inhibitor and detected an increased fraction of cells expressing βIII-tubulin and GFAP 4 days after treatment, as well as an

enhancement in FBS/RA-induced differentiation. Our data are thus in agreement with the view that prolonging G1 length increases the likelihood of commitment.

The standard *in vitro* culture conditions used here are different from the *in vivo* growth conditions of NSCs in the SVZ, where stem cells are mostly quiescent (Doetsch, 2003), whereas they become highly proliferative *in vitro* in the presence of abundant growth factors. Nevertheless, the capacity of cells to extensively self-renew and differentiate into three lineages are widely used criteria to define a NSC state (Conti and Cattaneo, 2010; Pastrana et al., 2011). These culture conditions are known to favour the expansion of both activated stem cells as well as transit-amplifying cells (TAPs) expressing the EGF receptor (Doetsch et al., 2002a; Pastrana et al., 2009). Our *in vitro* data show that the cell cycle kinetics determined by FUCCI (Fig. 7) match quite well with what was previously observed *in vivo*, where a cycle of about 18-24 hours was measured for activated stem cells and TAPs (Cameron and McKay, 2001; Doetsch et al., 1999; Hayes and Nowakowski, 2002). Under self-renewing conditions, the fast cycling cells, which correspond to the undifferentiated cells in the population, have a total average cell cycle of ~20 hours and a G1 below 15 hours.

Recent studies showed that the *in vitro* culture of freshly isolated SVZ-derived NSC in the absence of growth factors quite faithfully mimics the lineage differentiation pattern found *in vivo* (Costa et al., 2011). Slowly dividing astrocytes, representing the *in vivo* quiescent stem cell, would then give rise to faster proliferating astro/radial glia, then to TAPs and finally differentiate to neuroblasts. The cell cycle parameter of the fast dividing astro/radial glia cells with a cell cycle length of ~15 hours and their highly synchronous behaviour is in line with our findings. Therefore, we believe that whereas in the absence of growth factors this expansion phase is only temporally limited [five rounds of divisions were identified by Costa et al. (Costa et al., 2011)] and followed by terminal differentiation, in presence of growth factors this may be expanded through self-renewing divisions.

Single cell analysis and tracking of FUCCI-NSC allowed us to identify cell cycle parameters that correlate with the extent of differentiation. We used the accumulation of Cdt1-KO2 to distinguish between slow and fast cycling cells based on red fluorescence intensities. By analysing expression levels of several marker genes, we showed that the slow cycling cells express higher levels of differentiation markers, whereas fast cycling cells represent a population of more primitive cells. This was further confirmed by generating a Hes5::GFP-Cdt1-KO2 reporter line. In this system, the loss of GFP expression, which marks loss of stemness, was specifically associated with increased levels of red fluorescence, whereas high GFP-expressing cells showed higher percentage of S/G2-M cells compared with low GFP-expressing cells. This is in agreement with previous findings demonstrating higher clone-forming efficiency in the high GFP-expressing cells (Basak and Taylor, 2007; Roccio et al., 2012).

Fast cell cycle progression has previously been proposed as one hallmark of self-renewing mouse ESC that transit very quick through G1, presumably to avoid commitment signals and thus maintain a pluripotent state (Orford and Scadden, 2008; Singh and Dalton, 2009). Consistent with this notion, in mouse ESC transduced with the FUCCI reporter system, we measured average G1 lengths of only 2 hours with a cell cycle duration of ~14 hours. Conversely, G1 extended very rapidly upon differentiation.

Based on the cell cycle analysis of FUCCI-NSC and FUCCI-ESC, we hypothesised that early changes in cell cycle profile during the reprogramming of NSC to iPS cells could be identified using our platform. Previous work had shown that primary colonies originating from fibroblast reprogramming were derived from cells that were smaller in size and cycled faster than non-reprogramming neighbouring cells (Smith et al., 2010). Indeed, upon overexpression of the four reprogramming factors c-Myc, Klf4, Sox2 and Oct4, we detected the appearance of proliferating cells based on the expression of the green Gem-AG FUCCI reporter. These cells represent a minor fraction (4% at day 4) of the total cell population that would be difficult to identify by other means such as by conventional marker expression at this very early time point. By sorting green cells, we were able to further enrich the population of reprogramming cells. Although this was crucial to enable imaging at a single-cell level and to track proliferating colonies reminiscent of ESC colonies, further analyses are needed to prove that these clones will fully reprogram and to dissect how cell cycle parameters change during this transition.

NSC reprogramming has been previously shown to be more efficient than for mouse fibroblasts, based on the fact that these cells may represent an intermediate stage between fibroblasts and iPS cells (Kim et al., 2008). However, the selection of fast proliferating cells may also improve the efficiency for other cell types. Acceleration of cell cycle progression through inhibition of the p53/p21 pathway or ectopic expression of Lin28 increased the speed of conversion into iPS cells (e.g. Hanna et al., 2009). Moreover, besides the well-established role of c-Myc in promoting cell cycle progression (Singh and Dalton, 2009), a direct relationship between regulators of pluripotency and cell cycle has been described (Card et al., 2008; Lee et al., 2010; Zhang et al., 2009). Our findings therefore confirm previous observations suggesting that the cell cycle is a key parameter in iPS cell generation. Accelerated cell division could increase the probability of iPS cell generation and/or cell cycle-specific events such as DNA replication might be the prerequisite for permitting the epigenetic changes to occur. The analysis of reprogramming events using the FUCCI cell cycle reporter may help to elucidate this issue.

In conclusion, the systematic analysis of changes in cell cycle parameters during proliferative and differentiating cell divisions allowed us to identify traits that are indicative of the stem cell and more committed cell state, and that can be exploited to improve differentiation and reprogramming conditions. In combination with genetic tools and other reporter gene systems, our approaches should provide new avenues to address pertinent questions in stem cell biology.

Acknowledgements

We thank Mukul Girotra for help with animal breeding and genotyping; Jalil Zerdani and Raphaelle Luisier for initial work on the FUCCIJ plug-in; Celine Ruegsegger for help with the characterisation of FUCCI-NSC; Francois Gorostidi for providing the lentiviral vectors; members of the Flow Cytometry Core Facility of EPFL for support with sorting experiments; Sebastian Jessberger for experimental tools; Verdon Taylor for providing Hes5::GFP cells; and Rudolf Jaenisch for providing the polycistronic vectors for iPS cell generation.

Funding

This work was supported by a Marie Curie fellowship to M.R.; by a European Young Investigator (EURYI) Award [PE002-117115/1] to M.P.L.; and by Swiss National Science Foundation grants [CR32I3_125426 and CR23I2_125290].

Competing interests statement

The authors declare no competing financial interests.

Supplementary material

Supplementary material available online at
http://dev.biologists.org/lookup/suppl/doi:10.1242/dev.086215/-/DC1

References

Abrous, D. N., Koehl, M. and Le Moal, M. (2005). Adult neurogenesis: from precursors to network and physiology. *Physiol. Rev.* **85**, 523-569.

Arai, Y., Pulvers, J. N., Haffner, C., Schilling, B., Nüsslein, I., Calegari, F. and Huttner, W. B. (2011). Neural stem and progenitor cells shorten S-phase on commitment to neuron production. *Nat. Commun.* **2**, 154.

Artegiani, B., Lindemann, D. and Calegari, F. (2011). Overexpression of cdk4 and cyclinD1 triggers greater expansion of neural stem cells in the adult mouse brain. *J. Exp. Med.* **208**, 937-948.

Basak, O. and Taylor, V. (2007). Identification of self-replicating multipotent progenitors in the embryonic nervous system by high Notch activity and Hes5 expression. *Eur. J. Neurosci.* **25**, 1006-1022.

Beukelaers, P., Vandenbosch, R., Caron, N., Nguyen, L., Belachew, S., Moonen, G., Kiyokawa, H., Barbacid, M., Santamaria, D. and Malgrange, B. (2011). Cdk6-dependent regulation of G(1) length controls adult neurogenesis. *Stem Cells* **29**, 713-724.

Blomen, V. A. and Boonstra, J. (2007). Cell fate determination during G1 phase progression. *Cell. Mol. Life Sci.* **64**, 3084-3104.

Burdon, T., Stracey, C., Chambers, I., Nichols, J. and Smith, A. (1999). Suppression of SHP-2 and ERK signalling promotes self-renewal of mouse embryonic stem cells. *Dev. Biol.* **210**, 30-43.

Burdon, T., Smith, A. and Savatier, P. (2002). Signalling, cell cycle and pluripotency in embryonic stem cells. *Trends Cell Biol.* **12**, 432-438.

Calegari, F. and Huttner, W. B. (2003). An inhibition of cyclin-dependent kinases that lengthens, but does not arrest, neuroepithelial cell cycle induces premature neurogenesis. *J. Cell Sci.* **116**, 4947-4955.

Calegari, F., Haubensak, W., Haffner, C. and Huttner, W. B. (2005). Selective lengthening of the cell cycle in the neurogenic subpopulation of neural progenitor cells during mouse brain development. *J. Neurosci.* **25**, 6533-6538.

Cameron, H. A. and McKay, R. D. (2001). Adult neurogenesis produces a large pool of new granule cells in the dentate gyrus. *J. Comp. Neurol.* **435**, 406-417.

Card, D. A., Hebbar, P. B., Li, L., Trotter, K. W., Komatsu, Y., Mishina, Y. and Archer, T. K. (2008). Oct4/Sox2-regulated miR-302 targets cyclin D1 in human embryonic stem cells. *Mol. Cell. Biol.* **28**, 6426-6438.

Carey, B. W., Markoulaki, S., Hanna, J., Saha, K., Gao, Q., Mitalipova, M. and Jaenisch, R. (2009). Reprogramming of murine and human somatic cells using a single polycistronic vector. *Proc. Natl. Acad. Sci. USA* **106**, 157-162.

Conti, L. and Cattaneo, E. (2010). Neural stem cell systems: physiological players or *in vitro* entities? *Nat. Rev. Neurosci.* **11**, 176-187.

Cordey, M., Limacher, M., Kobel, S., Taylor, V. and Lutolf, M. P. (2008). Enhancing the reliability and throughput of neurosphere culture on hydrogel microwell arrays. *Stem Cells* **26**, 2586-2594.

Costa, M. R., Ortega, F., Brill, M. S., Beckervordersandforth, R., Petrone, C., Schroeder, T., Götz, M. and Berninger, B. (2011). Continuous live imaging of adult neural stem cell division and lineage progression *in vitro*. *Development* **138**, 1057-1068.

Doetsch, F. (2003). The glial identity of neural stem cells. *Nat. Neurosci.* **6**, 1127-1134.

Doetsch, F., García-Verdugo, J. M. and Alvarez-Buylla, A. (1999). Regeneration of a germinal layer in the adult mammalian brain. *Proc. Natl. Acad. Sci. USA* **96**, 11619-11624.

Doetsch, F., Petreanu, L., Caille, I., Garcia-Verdugo, J. M. and Alvarez-Buylla, A. (2002a). EGF converts transit-amplifying neurogenic precursors in the adult brain into multipotent stem cells. *Neuron* **36**, 1021-1034.

Doetsch, F., Verdugo, J. M., Caille, I., Alvarez-Buylla, A., Chao, M. V. and Casaccia-Bonnefil, P. (2002b). Lack of the cell-cycle inhibitor p27Kip1 results in selective increase of transit-amplifying cells for adult neurogenesis. *J. Neurosci.* **22**, 2255-2264.

Filipczyk, A. A., Laslett, A. L., Mummery, C. and Pera, M. F. (2007). Differentiation is coupled to changes in the cell cycle regulatory apparatus of human embryonic stem cells. *Stem Cell Res.* **1**, 45-60.

Fluckiger, A. C., Marcy, G., Marchand, M., Négre, D., Cosset, F. L., Mitalipov, S., Wolf, D., Savatier, P. and Dehay, C. (2006). Cell cycle features of primate embryonic stem cells. *Stem Cells* **24**, 547-556.

Giachino, C., Basak, O. and Taylor, V. (2009). Isolation and manipulation of mammalian neural stem cells *in vitro*. *Methods Mol. Biol.* **482**, 143-158.

Gobaa, S., Hoehnel, S., Roccio, M., Negro, A., Kobel, S. and Lutolf, M. P. (2011). Artificial niche microarrays for probing single stem cell fate in high throughput. *Nat. Methods* **8**, 949-955.

Götz, M. and Huttner, W. B. (2005). The cell biology of neurogenesis. *Nat. Rev. Mol. Cell Biol.* **6**, 777-788.

Hanna, J., Saha, K., Pando, B., van Zon, J., Lengner, C. J., Creyghton, M. P., van Oudenaarden, A. and Jaenisch, R. (2009). Direct cell reprogramming is a stochastic process amenable to acceleration. *Nature* **462**, 595-601.

Harbour, J. W., Luo, R. X., Dei Santi, A., Postigo, A. A. and Dean, D. C. (1999). Cdk phosphorylation triggers sequential intramolecular interactions that progressively block Rb functions as cells move through G1. *Cell* **98**, 859-869.

Hayes, N. L. and Nowakowski, R. S. (2002). Dynamics of cell proliferation in the adult dentate gyrus of two inbred strains of mice. *Brain Res. Dev. Brain Res.* **134**, 77-85.

Kim, J. B., Zaehres, H., Wu, G., Gentile, L., Ko, K., Sebastiano, V., Araúzo-Bravo, M. J., Ruau, D., Han, D. W., Zenke, M. et al. (2008). Pluripotent stem cells induced from adult neural stem cells by reprogramming with two factors. *Nature* **454**, 646-650.

Kim, J. B., Zaehres, H., Araúzo-Bravo, M. J. and Schöler, H. R. (2009). Generation of induced pluripotent stem cells from neural stem cells. *Nat. Protoc.* **4**, 1464-1470.

Kippin, T. E., Martens, D. J. and van der Kooy, D. (2005). p21 loss compromises the relative quiescence of forebrain stem cell proliferation leading to exhaustion of their proliferation capacity. *Genes Dev.* **19**, 756-767.

Kowalczyk, A., Filipkowski, R. K., Rylski, M., Wilczynski, G. M., Konopacki, F. A., Jaworski, J., Ciemerych, M. A., Sicinski, P. and Kaczmarek, L. (2004). The critical role of cyclin D2 in adult neurogenesis. *J. Cell Biol.* **167**, 209-213.

Kriegstein, A. and Alvarez-Buylla, A. (2009). The glial nature of embryonic and adult neural stem cells. *Annu. Rev. Neurosci.* **32**, 149-184.

Lange, C. and Calegari, F. (2010). Cdks and cyclins link G1 length and differentiation of embryonic, neural and hematopoietic stem cells. *Cell Cycle* **9**, 1893-1900.

Lange, C., Huttner, W. B. and Calegari, F. (2009). Cdk4/cyclinD1 overexpression in neural stem cells shortens G1, delays neurogenesis, and promotes the generation and expansion of basal progenitors. *Cell Stem Cell* **5**, 320-331.

Lee, J., Go, Y., Kang, I., Han, Y. M. and Kim, J. (2010). Oct-4 controls cell-cycle progression of embryonic stem cells. *Biochem. J.* **426**, 171-181.

Lugert, S., Basak, O., Knuckles, P., Haussler, U., Fabel, K., Götz, M., Haas, C. A., Kempermann, G., Taylor, V. and Giachino, C. (2010). Quiescent and active hippocampal neural stem cells with distinct morphologies respond selectively to physiological and pathological stimuli and aging. *Cell Stem Cell* **6**, 445-456.

Ohtsuka, S. and Dalton, S. (2008). Molecular and biological properties of pluripotent embryonic stem cells. *Gene Ther.* **15**, 74-81.

Orford, K. W. and Scadden, D. T. (2008). Deconstructing stem cell self-renewal: genetic insights into cell-cycle regulation. *Nat. Rev. Genet.* **9**, 115-128.

Pastrana, E., Cheng, L. C. and Doetsch, F. (2009). Simultaneous prospective purification of adult subventricular zone neural stem cells and their progeny. *Proc. Natl. Acad. Sci. USA* **106**, 6387-6392.

Pastrana, E., Silva-Vargas, V. and Doetsch, F. (2011). Eyes wide open: a critical review of sphere-formation as an assay for stem cells. *Cell Stem Cell* **8**, 486-498.

Roccio, M., Gobaa, S. and Lutolf, M. P. (2012). High-throughput clonal analysis of neural stem cells in microarrayed artificial niches. *Integr. Biol.* **4**, 391-400.

Sakaue-Sawano, A., Kurokawa, H., Morimura, T., Hanyu, A., Hama, H., Osawa, H., Kashiwagi, S., Fukami, K., Miyata, T., Miyoshi, H. et al. (2008). Visualizing spatiotemporal dynamics of multicellular cell-cycle progression. *Cell* **132**, 487-498.

Sakaue-Sawano, A., Kobayashi, T., Ohtawa, K. and Miyawaki, A. (2011). Drug-induced cell cycle modulation leading to cell-cycle arrest, nuclear mis-segregation, or endoreplication. *BMC Cell Biol.* **12**, 2.

Salomoni, P. and Calegari, F. (2010). Cell cycle control of mammalian neural stem cells: putting a speed limit on G1. *Trends Cell Biol.* **20**, 233-243.

Savatier, P., Huang, S., Szekely, L., Wiman, K. G. and Samarut, J. (1994). Contrasting patterns of retinoblastoma protein expression in mouse embryonic stem cells and embryonic fibroblasts. *Oncogene* **9**, 809-818.

Singh, A. M. and Dalton, S. (2009). The cell cycle and Myc intersect with mechanisms that regulate pluripotency and reprogramming. *Cell Stem Cell* **5**, 141-149.

Smith, Z. D., Nachman, I., Regev, A. and Meissner, A. (2010). Dynamic single-cell imaging of direct reprogramming reveals an early specifying event. *Nat. Biotechnol.* **28**, 521-526.

Stead, E., White, J., Faast, R., Conn, S., Goldstone, S., Rathjen, J., Dhingra, U., Rathjen, P., Walker, D. and Dalton, S. (2002). Pluripotent cell division cycles are driven by ectopic Cdk2, cyclin A/E and E2F activities. *Oncogene* **21**, 8320-8333.

Takahashi, T., Nowakowski, R. S. and Caviness, V. S., Jr (1995). The cell cycle of the pseudostratified ventricular epithelium of the embryonic murine cerebral wall. *J. Neurosci.* **15**, 6046-6057.

Zhang, X., Neganova, I., Przyborski, S., Yang, C., Cooke, M., Atkinson, S. P., Anyfantis, G., Fenyk, S., Keith, W. N., Hoare, S. F. et al. (2009). A role for NANOG in G1 to S transition in human embryonic stem cells through direct binding of CDK6 and CDC25A. *J. Cell Biol.* **184**, 67-82.

Zhu, G., Conner, S. E., Zhou, X., Shih, C., Li, T., Anderson, B. D., Brooks, H. B., Campbell, R. M., Considine, E., Dempsey, J. A. et al. (2003). Synthesis, structure-activity relationship, and biological studies of indolocarbazoles as potent cyclin D1-CDK4 inhibitors. *J. Med. Chem.* **46**, 2027-2030.